11-2006

The Role of a Conserved Serine Residue within Hydrogen Bonding Distance of FAD in Redox Properties and the Modulation of Catalysis by Ca2+/Calmodulin of Constitutive Nitric-oxide Synthases

Satya Prakash Panda
University of Texas at San Antonio

Ying Tong Gao
University of Texas at San Antonio

Linda J. Roman
University of Texas at San Antonio

Pavel Marta´sek
Charles University School of Medicine

John C. Salerno
Kennesaw State University, jsalern3@kennesaw.edu

Recommended Citation
Panda SP, Gao YT, Roman LJ, Marta´sek P, Salerno JC, Masters BSS. 2006. The role of a conserved serine residue within hydrogen bonding distance of FAD in redox properties and the modulation of catalysis by Ca2+/calmodulin of constitutive nitric-oxide synthases. J Biol Chem. 281(45):34246-57.

See next page for additional authors

THE JOURNAL OF BIOLOGICAL CHEMISTRY VOL. 281, NO. 45, pp. 34246–34257, November 10, 2006

The Role of a Conserved Serine Residue within Hydrogen Bonding Distance of FAD in Redox Properties and the Modulation of Catalysis by Ca^{2+}/Calmodulin of Constitutive Nitric-oxide Synthases*

Received for publication, February 2, 2006, and in revised form, August 10, 2006 Published, JBC Papers in Press, September 11, 2006, DOI 10.1074/jbc.M601041200

Satya Prakash Panda[‡], Ying Tong Gao[‡], Linda J. Roman[‡], Pavel Martásek[‡§], John C. Salerno[¶], and Bettie Sue S. Masters[‡1]

From the [‡]Department of Biochemistry, The University of Texas Health Science Center at San Antonio, San Antonio, Texas 78229-3900, the [¶]Department of Biological and Physical Sciences, College of Science and Mathematics, Kennesaw State University, Kennesaw, Georgia 30144, and the [§]Department of Pediatrics, Charles University School of Medicine I, Prague 2 21, Czech Republic

The crystal structure of the neuronal nitric-oxide synthase (nNOS) NADPH/FAD binding domain indicated that Ser-1176 is within hydrogen bonding distance of Asp-1393 and the O4 atom of FAD and is also near the N5 atom of FAD (3.7 Å). This serine residue is conserved in most of the ferredoxin-$NADP^+$ reductase family of proteins and is important in electron transfer. In the present study, the homologous serines of both nNOS (Ser-1176) and endothelial nitric-oxide synthase (eNOS) (Ser-942) were mutated to threonine and alanine. Both substitutions yielded proteins that exhibited decreased rates of electron transfer through the flavin domains, in the presence and absence of Ca^{2+}/CaM, as measured by reduction of potassium ferricyanide and cytochrome *c*. Rapid kinetics measurements of flavin reduction of all the mutants also showed a decrease in the rate of flavin reduction, in the absence and presence of Ca^{2+}/CaM, as compared with the wild type proteins. The serine to alanine substitution caused both nNOS and eNOS to synthesize NO more slowly; however, the threonine mutants gave equal or slightly higher rates of NO production compared with the wild type enzymes. The midpoint redox potential measurements of all the redox centers revealed that wild type and threonine mutants of both nNOS and eNOS are very similar. However, the redox potentials of the FMN/$FMNH^{\cdot}$ couple for alanine substitutions of both nNOS and eNOS are >100 mV higher than those of wild type proteins and are positive. These data presented here suggest that hydrogen bonding of the hydroxyl group of serine or threonine with the isoalloxazine ring of FAD and with the amino acids in its immediate milieu, particularly nNOS Asp-1393, affects the redox potentials of various flavin states, influencing the rate of electron transfer.

Nitric-oxide synthases (NOSs)[2] are bidomain enzymes, with an N-terminal heme or oxygenase domain and a C-terminal flavin or reductase domain connected by a calmodulin (CaM) binding region. These enzymes catalyze the conversion of L-arginine to nitric oxide (NO) and L-citrulline in a series of two monooxygenase reactions (1, 2). Upon binding of Ca^{2+}/CaM, electrons donated by NADPH are passed through the reductase domain to the heme domain, where NO is formed. NO plays an important role in both the physiology and pathology of many organisms, including humans (3). NO is produced in a cell- and tissue-specific manner by three different isoforms, namely neuronal NOS (nNOS), endothelial NOS (eNOS) and inducible NOS (iNOS), which are encoded by three different genes. Both nNOS and eNOS are expressed constitutively, whereas iNOS expression is regulated at the transcriptional level by cytokines and interleukins. An influx of calcium into the cell is necessary for CaM to bind to constitutive NOSs, whereas it is tightly bound to iNOS (4). The rates of electron transfer and NO production vary among the three isoforms.

Crystal structures of the heme domain dimers of nNOS (5, 6), eNOS (7, 8), and iNOS (8, 9) have been solved. All three enzymes showed a similar α/β fold with a single zinc atom per dimer (7, 8), and all maintained similar topologies of binding for substrate and cofactors. So far, no substantial difference has been found among the heme domains that can explain the variance among the activities of NOS isoforms. The reductase domains of all NOSs bear ~50–60% sequence similarity with NADPH-cytochrome P450 oxidoreductase (CYPOR) (10). Primary sequence comparison revealed the presence of a stretch of ~45 amino acids in the FMN binding domain of constitutive NOSs that is absent in iNOS and CYPOR (11). This stretch of amino acids, known as the autoregulatory insert, regulates the flow of electrons in a Ca^{2+}/CaM-dependent manner. The C-terminal ends of all three isoforms, which are absent in CYPOR, are also calmodulin-modulated regulatory regions (12–15). These C-terminal tails negatively modulate the flow of electrons through the reductase domain in the absence of

* This work was supported by National Institutes of Health Grants GM52419 and HL30050 and Robert A. Welch Foundation Grant AQ1192 (to B. S. S. M.) and partially supported by Czech Granting Agency Grant GACR 303/05/0336 (to P. M.). This work represents partial fulfillment of the requirement for the Doctor of Philosophy degree at The University of Texas Health Science Center at San Antonio (S. P. P.). The costs of publication of this article were defrayed in part by the payment of page charges. This article must therefore be hereby marked "*advertisement*" in accordance with 18 U.S.C. Section 1734 solely to indicate this fact.

[1] To whom correspondence should be addressed: Dept. of Biochemistry, The University of Texas Health Science Center at San Antonio, 7703 Floyd Curl Dr., San Antonio, TX 78229. Tel.: 210-567-6627; E-mail: masters@uthscsa.edu.

[2] The abbreviations used are: NOS, nitric-oxide synthase; nNOS, neuronal nitric-oxide synthase; eNOS, endothelial nitric-oxide synthase; iNOS, inducible nitric-oxide synthase; NO, nitric oxide; CaM, calmodulin; CYPOR, cytochrome P450 oxidoreductase.

Ca^{2+}/CaM. These findings suggest that electron flux is regulated to a large extent by various intrinsic elements present in the reductase domain of the NOSs.

Initially, the structure of the soluble portion of CYPOR, which possesses ~50–60% sequence similarity with the NOS reductase domains, presented a prototype for the overall folds of the reductase domains and the relative positioning of FAD, FMN, and NADP(H) in these NOS isoforms (16). The solution of crystal structures of a fragment of the nNOS reductase domain, containing the NADPH binding site and the connecting/FAD binding domain (17), and the nNOS reductase domain, containing both FAD and FMN binding domains (18), demonstrated that the three-dimensional folds of the nNOS reductase domain and CYPOR are highly conserved. The similarities of the NOS reductase domains and CYPOR, as well as their general electron transferring properties, permitted predictions of important amino acid residues in the NOSs based on their importance in CYPOR (19–23). For example, mutation of serine 457 of rat CYPOR inhibits the rate of electron transfer from CYPOR to external electron acceptors, such as cytochrome *c*, and affects the redox potentials of the bound flavins (22). This serine, which is located near the FAD in both nNOS and CYPOR, within hydrogen bonding distance of the isoalloxazine ring, is conserved across flavoprotein reductases (24). In the present study, the homologous serine residues of both nNOS (Ser-1176) and eNOS (Ser-942) have been mutated to either threonine or alanine in an attempt to understand the role of hydrogen bonding by this residue in electron transfer and its effect on redox potentials in the cNOSs (nNOS and eNOS). Due to the autoregulatory inserts in the sequences of the NOS flavoprotein domains and the role of Ca^{2+}/CaM for the activities, the consequences of such substitutions could *not* be assumed to be predictable. Substitution of serine by threonine was chosen because the threonine residue has an additional methylene group as compared with serine but retains the -OH group and, thus, may not disrupt the hydrogen bonding network in the region. With the alanine substitution, however, disruption of the hydrogen bonding network occurs, since alanine lacks the -OH group. Substitution of serine by either alanine or threonine in nNOS and eNOS inhibited the rate of reduction of both potassium ferricyanide and cytochrome *c*. On the other hand, the threonine mutants of both nNOS and eNOS showed equal or slightly increased NO production as compared with the wild type protein. The redox potentials of different redox centers of wild type and mutant proteins were also measured, and differences were found for the alanine-substituted proteins but not for the threonine mutant as compared with the respective wild type proteins. The implications of these results in the overall mechanisms of the constitutive NOS isoforms are discussed.

EXPERIMENTAL PROCEDURES

Chemicals/Enzymes—Trizma base, L-arginine, cytochrome *c* (horse heart), $K_3Fe(CN)_6$, and other basic chemicals were obtained from Sigma. NADPH was purchased from Alexis (San Diego, CA). Tetrahydrobiopterin was from Research Biochemicals International (Natick, MA) or from Sigma. PfuTurbo polymerase and XL10 Gold *Escherichia coli* cells were purchased from Stratagene (La Jolla, CA). Restriction enzymes were from either Promega (Madison, WI) or New England Biolabs (Beverly, MA).

DNA Primers and Sequencing—Synthesis of all the nucleotide primers and sequencing of all clones were performed in the Center for Advanced DNA Technologies at the University of Texas Health Science Center at San Antonio, an institutional core facility.

Site-directed Mutagenesis—eNOS S942A and S942T were created by a three-primer technique, where a primer containing the desired mutation is phosphorylated and incorporated during PCR amplification (25). The mutational primers were phosphorylated during synthesis: upstream, aca tct tca gcc ccc aaa cgg a; downstream, tgg ttg ccat agt gac atc. Phosphorylated primers were gca gcc ccg gac tac act gtc agc tcg gcc ccc aac gcc ca (S942T) and gca gcc ccg gac tac gct gtc agc tcg gcc ccc aac gcc ca (S942A).

A polymerase chain reaction was carried out using three primers (upstream, downstream, and phosphorylated primers) and Bov-eNOSpCW as template (26). The 1.2-kb PCR-amplified product, which contained two unique restriction sites, KpnI and XhoI, and the desired mutation, was gel-purified. In two independent reactions, this gel-purified 1.2-kb DNA piece, along with Bov-eNOSpCW, was digested with KpnI and XhoI. The larger piece from eNOS plasmid digestion was purified from a 1% agarose gel and ligated with the digested 1.2-kb PCR fragment. The ligated product was transformed into *E. coli* XL10 Gold cells (Stratagene) and grown on LB agar plates containing 50 μg/ml ampicillin. Preliminary screening was done by restriction digestion, and the mutations were confirmed by DNA sequencing. The plasmid containing the desired sequence was then transformed via electroporation into *E. coli* BL21 cells for protein expression.

nNOS S1176A and S1176T were produced by two sequential PCR amplifications. Two complementary primers were designed containing the codon for the desired mutations. Two additional primers, sense and antisense, were designed to amplify the entire nNOS coding region of nNOSpCW (27), including the restriction sites NdeI and XbaI, at the 5′ and 3′ end, respectively. In the first PCR amplification, the 5′ and 3′ regions were amplified separately, using the nNOSpCW as a template, with one middle primer and one end primer. The middle primer contained the codon for the desired mutation. In the second PCR, products of the first PCR amplification were used as templates, and the end primers were used, incorporating NdeI and XbaI sites for insertion into the pCW vector. The second PCR product was digested with NdeI and XbaI before ligating to the pCWori vector digested with the same restriction enzymes. The ligated product was transformed into *E. coli* XL10 Gold cells (Stratagene) and grown on agar plates containing 50 μg/ml ampicillin. Mutations were confirmed by DNA sequencing. The plasmid containing the desired sequence was then transformed via electroporation into *E. coli* BL21 cells for protein expression.

First PCR—nNOS 5′ region amplification primers were as follows: sense/upstream primer (NdeI restriction site), gca tgc cat atg gct gaa gag aac acg ttt ggg; downstream (middle primer containing the mutational codon), S1176T (gga gct gat ggt gta gta gcg agg ctg cag) and S1176A (gga gct gat ggc gta gta gcg agg

ctg cag). NOS 3′ region amplification primers were as follows: upstream (middle primer containing the codon for desired mutation), S1176T (cgc tac tac acc atc agc tcc tct cag ac) and S1176A (cgc tac tac cgc atc agc tcc tct cag ac); antisense/downstream primer (XbaI restriction site), atg cat tct aga tta gga gct gaa aac ctc atc.

Second PCR—Sense/upstream primer (NdeI restriction site) was gca tgc cat atg gct gaa gag aac acg ttt ggg. Antisense/downstream primer (XbaI restriction site) was atg cat tct aga tta gga gct gaa aac ctc atc.

Protein Expression and Purification—All the NOSs (wild type and mutants) were purified as published (26, 27). Calmodulin was expressed and purified according to Zhang and Vogel (28).

Measurement of Heme and Flavin Content—The total heme content was measured by the pyridine hemochromogen method as previously described (29, 30). In short, the protein was incubated in 0.1 N NaOH and 30% pyridine, and the pyridine hemochromogen spectrum was obtained. Concentration of heme was calculated using the extinction coefficient, $\epsilon = 34$ mM^{-1} cm^{-1} at 556 nm.

The FAD and FMN contents of wild type and mutant proteins were measured as described by Faeder and Siegel (31). In short, known amounts of protein samples were boiled for 5 min and centrifuged for 10 min to pellet the precipitated protein. Aliquots of supernatant, which contained FAD and FMN, were taken, and the fluorescence was measured at two different pH states to differentiate between the flavins. Concentrations of FAD and FMN were calculated by comparison with standard curves, as described (31). The flavin content of these enzymes was also measured using a high pressure liquid chromatography method. Samples were diluted to a final concentration of 1 μM in distilled H_2O and boiled for 5 min and spun for 10 min at high speed before injecting into a C18 column under isocratic flow of 10 mM $(NH_4)_2HPO_4$, pH 5.5, and CH_3CN in a ratio of 100:12. The FAD and FMN contents were determined by comparing the percentage of area under the peak with the standards (32).

Reductase Activities—Cytochrome *c* reduction by these proteins was measured as described by Masters *et al.* (33) with modification. In short, the rate of cytochrome *c* reduction was measured as the rate of increase in absorbance at 550 nm using the molar extinction coefficient 21 mM^{-1} cm^{-1}. The reaction was performed in 50 mM Tris/HCl buffer, pH 7.4, with 100 mM NaCl and 40 μM cytochrome *c*, 10–50 nM enzyme, a 5–7.5-fold molar excess of CaM to the enzyme, 200 μM $CaCl_2$, and 100 μM NADPH. The reactions were monitored for 30 s, and the initial rates were plotted. Determination of K_m for cytochrome *c* involved variation of cytochrome *c* concentration from 1 to 50 μM. The range of NADPH concentration used was 250 nM to 50 μM for the K_m determination of NADPH, keeping the cytochrome *c* concentration at 40 μM.

Potassium ferricyanide ($K_3Fe(CN)_6$) reduction was measured as the rate of decrease in absorbance at 420 nm over 30 s, using a molar extinction coefficient of 1.02 mM^{-1} cm^{-1}. The amounts of enzyme, calmodulin, and NADPH used were the same as those used in the cytochrome *c* reduction assays. The concentration of $K_3Fe(CN)_6$ used was varied from 0.025 to 3.0 mM for each rate calculation. The measured turnover numbers were plotted against the concentrations of $K_3Fe(CN)_6$, for determination of K_m for ferricyanide, and the turnover number was determined by fitting the data using the Michaelis-Menten equation. All steady-state spectrophotometric measurements were performed on a Shimadzu model 2401PC UV-visible dual beam spectrophotometer.

Rapid Kinetics Measurement of Flavin Reduction—The rate of flavin reduction was measured as described (34) using an Applied Photophysics SX.18MV stopped-flow spectrophotometer. Measurements were carried out using 2 μM enzyme, 100 μM NADPH, without or with 10 μM calmodulin, and an excess of $CaCl_2$ in 50 mM Tris/HCl, pH 7.4, and 100 mM NaCl. The rate of flavin reduction was monitored at 485 nm for 0.5 or 2.0 s, and the reduction rates were calculated by fitting the data to a double exponential equation, which fitted the rate data best, using vendor-supplied software. The rates are expressed as s^{-1}.

Nitric Oxide Formation—The rate of NO production was measured as the rate of formation of methemoglobin from oxyhemoglobin upon the binding of NO, as described (35). The reaction mixture contained 8 μM oxyhemoglobin, 100 μM L-arginine, 5 μM tetrahydrobiopterin, 100 μM NADPH, 25–50 nM enzyme, 187.5–375 nM calmodulin, and 200 μM $CaCl_2$ in 50 mM Tris/HCl, pH 7.4, and 100 mM NaCl. The reaction was monitored as a change in absorbance at 401 nm, and rates were calculated using the extinction coefficient 60 mM^{-1} cm^{-1}.

Potentiometric Titrations—Redox titrations for both the wild types and their mutant enzymes were carried out as described by Dutton (36). All titrations were performed under nitrogen in a cuvette modified to accommodate the platinum/calomel combination reference electrode, which did not interfere with spectral measurements. All potentiometric experiments were performed at room temperature (23 °C as measured in the spectrophotometer). These titrations necessitate the repetitive removal of the cuvette from the instrument as each aliquot of reductant is delivered and subsequent mixing of the dyes on a miniature stir plate. Dye mediators used were methyl viologen (5 μM), benzyl viologen (5 μM), safranine o (2 μM), anthroquinone-2-sulfonate (10 μM), anthroquinone 2,6-disulfonate (10 μM), resorufin (2 μM), phenazine (5 μM), and 1,4-hydroxynaphthoquinone (5 μM) with dithionite as the reductant and potassium ferricyanide as the oxidant. Titrations of optical bands were simulated using the equations described by Gao *et al.* (37) and Dunford *et al.* (38).

Simulation of the optical bands was carried out by using summed contributions from heme states (two states) and flavin states (six states). At a given wavelength, these contributions are of the following form.

$$A_{\text{heme ox}} = C_{\text{heme}} \times \epsilon_{\text{heme ox}} \times 10^{(Eh - E_{\text{mheme}})\,F/RT}/(1 + 10^{(Eh - E_{\text{mheme}})\,F/RT}) \quad \text{(Eq. 1)}$$

$$A_{\text{heme red}} = C_{\text{heme}} \times \epsilon_{\text{heme red}} \times 10^{(Eh - E_{\text{mheme}})\,F/RT}/(1 + 10^{(Eh - E_{\text{mheme}})\,F/RT}) \quad \text{(Eq. 2)}$$

$$A_{\text{FAD}} = C_{\text{FAD}} \times \epsilon_{\text{FAD}} \times 1/(1 + 10^{(Eh - E_1\text{FAD})\,F/RT} + 10^{(Eh - E_1\text{FAD})\,F/RT}10^{(Eh - E_2\text{FAD})\,F/RT}) \quad \text{(Eq. 3)}$$

$$A_{FADH^{\cdot}} = C_{FAD} \times \epsilon_{FADH^{\cdot}} \times 10^{(Eh - E_1FAD)\,F/RT}/(1 + 10^{(Eh - E_1FAD)\,F/RT} + 10^{(Eh - E_1FAD)\,F/RT}10^{(Eh - E_2FAD)\,F/RT}) \quad \text{(Eq. 4)}$$

$$A_{FADH2} = C_{FAD} \times \epsilon_{FADH2} \times 10^{(Eh - E_1FAD)\,F/RT}10^{(Eh - E_2FAD)\,F/RT}/(1 + 10^{(Eh - E_1FAD)\,F/RT} + 10^{(Eh - E_1FAD)\,F/RT}10^{(Eh - E_2FAD)\,F/RT}) \quad \text{(Eq. 5)}$$

The value of RT/F at 25 °C is ~59.6 mV, and A represents the absorbance of different components. ϵ represents the extinction coefficient of the various redox states, with the subscript designating the redox state of a redox center. Variables of the form C_{heme} represent the total concentration of heme, which includes all of the redox and spin states (or, equivalently, flavin). These states are in rapid equilibrium during the time scale of redox equilibration in the experiment. *Eh* is the standard potential relative to the hydrogen electrode as measured potentiometrically. E_{mheme}, E_1FAD, and E_2FAD are the midpoint potentials of the one-electron couples. E_1 and E_2 are the midpoint potentials for the first and second one-electron reduced states. The absorbances associated with different redox states of FMN during titration are obtained by simply substituting FMN in place of FAD in Equations 3–5. In some cases, multiple heme components that differ in concentration, extinction coefficient, and midpoint potential have been introduced for simulation purposes.

Pure dye spectra were subtracted from the experimental spectra to derive the true change in the absorbance during titration. Spectra were further normalized for dilution and corrected for base line. Corrected absorbance at a given wavelength is plotted against the potential. Wavelengths were chosen at which the extinction coefficients of species of interest are dominant while other states are negligible. Theoretical curves were generated by manipulating parameters, such as midpoint potential (E_m) for each chromophore and amplitude, a term that includes both enzyme concentration and extinction coefficient at the corresponding wavelength, in each equation to fit the experimental data. For the simulation, the same extinction coefficient for FAD and FAD semiquinone and a 1:2 heme/flavin ratio were assumed. A value for the potential is accepted as the determined value when simulations at different wavelengths yield the same set of potentials.

The possibility of assigning more than one redox state to the data at a particular wavelength and the instability of some redox states that reduces the accumulation of the chromophore lead to uncertainty in the determination of some potentials; however, the confidence level of such assignments is determined from data at different wavelengths.

Flavin Reduction and Reoxidation—The reoxidation of flavin was monitored as a change in absorbance at 485 nm in the presence of 1 μM enzyme, 100 μM NADPH, without or with Ca^{2+}/CaM, in 50 mM Tris/HCl, pH 7.4, buffer, containing 100 mM NaCl. The reaction was initiated with fully oxidized enzyme, and NADPH was added after 60 s of monitoring the absorbance. The reaction was continued until no further net change in absorbance was observed (12, 13).

Rat nNOS	1164LTQLSLLQPRYY**S**ISSSPD.
Bovine eNOS	930LTQLPLLQPRYY**S**VSSAP..
Macrophage iNOS	891LSQLPILKPRYY**S**ISSSQD.
BM3	820~ALLPSIRPRYY**S**ISSSPR.
CYPOR	458CELLPRLQARYY**S**IASSSK.
Cytochrome b5 reductase	82TRIDGNLVIRPY**T**PVSSD..
Spinach FNR	139DKNGKPHKLRLY**S**IASSALG
Methionine Synthase Reductase	469LEHLPKLQPRPY**S**CASSSL.
Tobacco Nitrate Reductase	690AVIDDKLCMRAY**T**PTSTID.
E. coli Sulfite Reductase	377INLLRPLTPRLY**S**IASSQAE
Human NADPH Oxidase	329CPSISLLEWHPF**T**LTSAP..
Yeast Ferric Reductase	472~~PLYFWQSHPF**T**VLDSVSK

FIGURE 1. **Sequence alignments.** The accession number of each protein is given in italics within parentheses after each protein along with the relevant reference. Amino acid sequences of rat nNOS (*P29476*) (10), bovine eNOS (*P29473*) (56), macrophage iNOS (*NP_035057*) (57), CYP 102 (BM3) (*AAA87602*) (58), CYPOR (*NP_032924*) (59), rat cytochrome b_5 reductase (*NP_620232*) (60), ferredoxin reductase (spinach FNR) (*P00455*) (51), human methionine synthase reductase (*NP_076915*) (61), tobacco nitrate reductase (*CAA32217*) (62), *E. coli* sulfite reductase (*BAB37042*) (63), human NADPH oxidase (*NP_008983*) (64), and yeast ferric reductase (*NP_012702*) (65) were aligned using Bio-edit. Approximately 20 C-terminal amino acids of nNOS and the corresponding residues of other isoforms around the conserved serine residue (shown *boldface type*) are shown for clarity. ~ and ·, gaps during alignment.

RESULTS

Sequence Alignments and Structure Showing nNOS Ser-1176—The reductase domains of NOSs are members of the FAD/FMN-containing flavoprotein family with ~55% sequence similarity to CYPOR (10). The most conserved regions of this family of proteins are the NADPH-, FAD-, and FMN-binding sites (16). Fig. 1 shows a partial amino acid sequence alignment among the reductase domains of rat nNOS, bovine eNOS, macrophage iNOS, *Bacillus megaterium* CYP102 (P450 BM3), and other flavoproteins. A serine residue in the FAD binding domain (*boldface type* in Fig. 1) is one of the conserved residues in the flavoprotein family. Mutational studies of this conserved serine residue have been carried out for several of these flavoproteins. In the case of FNR, this conserved serine residue is primarily involved in hydride ion transfer by affecting the interaction between the nicotinamide ring of $NADP^+$ and FAD (39). In cytochrome b_5 reductase, the threonine residue at this position plays an important role in catalysis and electron transfer (40). The intricate hydrogen bonding network of this serine residue, along with conserved cysteine, aspartate, and tryptophan residues in CYPOR (16), has been implicated in hydride ion transfer in CYPOR (41).

Based on the crystal structures of the nNOS reductase domain and a fragment containing the NADPH- and FAD-binding domains, Ser-1176 of nNOS is near the N5 atom of the isoalloxazine ring of FAD (3.7 Å) and within hydrogen bonding distance of the FAD O4 atom (17, 18) (Fig. 2), suggesting a mechanistic role for this residue in NOSs also. Since electron flow through the reductase domain in the NOSs is regulated by CaM binding and by intrinsic protein elements, unlike any of the other flavoproteins listed, the role of this serine residue may be different or more complex (42). We mutated this conserved serine in both nNOS and eNOS to threonine, which appears in some flavoproteins at this site (Fig. 1), and to alanine.

To ascertain whether the purified mutant proteins were as stable as their wild type counterparts and contained similar amounts of prosthetic groups, the absolute spectra were compared, and heme and flavin contents of these proteins were

measured. All of the mutants contained amounts of heme, FAD, and FMN comparable with those of the wild type proteins and showed no differences in their absolute spectra (Fig. 3).

Reductase Activities of NOSs Using External Electron Acceptors—The location of this serine residue near the FAD in NOS isoforms and its putative participation in a hydrogen bonding network make it a good candidate for a role in electron transfer. To determine its influence on electron shuttling within the reductase domain, the rates of electron transfer to external acceptors, such as cytochrome *c* and potassium ferricyanide, were measured for the wild type proteins and compared with the threonine and alanine mutants. These measurements reflect the rate of electron transfer in the reductase domain from NADPH through FAD to FMN or through FAD alone, depending upon the specific acceptors involved. Cytochrome *c* reduction measures the rate of electron transfer through the entire reductase domain, since this acceptor receives electrons from FMN. Potassium ferricyanide reduction primarily reflects the rate of electron flow from NADPH through FAD, since potassium ferricyanide accepts electrons directly from FAD, analogous to CYPOR (42–45).

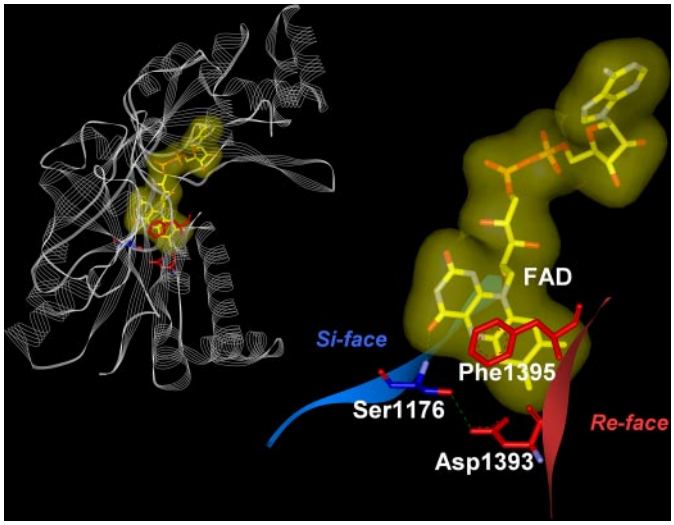

FIGURE 2. **Partial structure of nNOS reductase domain.** The figure shows Ser-1176 in *blue*, Asp-1393 and Phe-1395 in *red*, and space-filled FAD in *yellow* and partial backbone structure associated with these amino acids. The carbon backbone chain is shown as *flat ribbons*; *blue* is in the si-face, and *red* is in the re-face of the FAD. The partial backbone structure was shown in order to illustrate the bonding pattern between Ser-1176 and Asp-1393 of two different backbone chains. *Inset*, nNOS reductase domain structure (17, 18) spanning residues 963–1407.

Cytochrome c Reduction—Comparison of the rate of reduction of cytochrome *c* by nNOS and eNOS and their S1176T and S1176A mutants is shown in Fig. 4*a*. In the case of nNOS S1176T, the rate of cytochrome *c* reduction is decreased ~7–8-fold in the absence of Ca^{2+}/CaM (470 *versus* 60 min^{-1}) and is similarly decreased ~7–8-fold in the presence of Ca^{2+}/CaM (4777 *versus* 704 min^{-1}) as compared with that of wild type. The nNOS S1176A mutation lowered the rate of cytochrome *c* reduction 13-fold in the absence of Ca^{2+}/CaM (470 min^{-1} *versus* 36 min^{-1}) and 36-fold in the presence of Ca^{2+}/CaM (4777 *versus* 156 min^{-1}) in comparison with wild type protein.

The rate of electron transfer by eNOS is the slowest among the three NOS isoforms (46). Substitution of threonine for Ser-942 lowered the rate of electron transfer to cytochrome *c* ~2-fold both in the absence (243 *versus* 123 min^{-1}) and presence of Ca^{2+}/CaM (762 *versus* 431 min^{-1}) (Fig. 4*a*). The S942A substitution of eNOS inhibited the rate of cytochrome *c* reduction 10.5-fold in the absence (243 *versus* 23.2 min^{-1}) and ~7-fold in the presence of Ca^{2+}/CaM (762 *versus* 111 min^{-1}). Despite the fact that the threonine mutants showed a net decrease in the rate of cytochrome *c* reduction both in the absence and presence of Ca^{2+}/CaM, the stimulation of the reductase activity upon the addition of Ca^{2+}/CaM was the same as that of the wild type enzymes, which was not the case with alanine mutants.

The K_m values for cytochrome *c* for mutants were comparable with the wild type proteins (~3 μM), which suggests that the attenuation in the rate of cytochrome *c* reduction was not caused by alteration of cytochrome *c* interaction. Similarly, little or no difference was observed in the K_m value for NADPH between wild type and mutants of either nNOS or eNOS (0.15-0.5 μM), suggesting that the decrease in the reductase activity cannot be attributed to it.

Potassium Ferricyanide Reduction—The decreased rate of cytochrome *c* reduction implied that the electron flow to FMN was decreased as compared with the wild type protein. This inhibition of electron flow may occur at one or more of the following steps: NADPH → FAD, FAD → FMN, or FMN → cytochrome *c*. To determine whether the mutations affect electron transfer through FAD from NADPH, the rate of potassium ferricyanide reduction was measured for wild type proteins and for all of the mutants, since potassium ferricyanide can accept electrons from FAD (Fig. 4*b*). In the case of nNOS S1176T, a ~5-fold decrease from wild-type was observed in the absence of Ca^{2+}/CaM (wild type rate 38,000 min^{-1} *versus* mutant rate 7800 min^{-1}), and a similar -fold decrease (~5-fold) was observed in the presence of Ca^{2+}/CaM (wild type activity 48,000 min^{-1} *versus* mutant activity 9400 min^{-1}). A

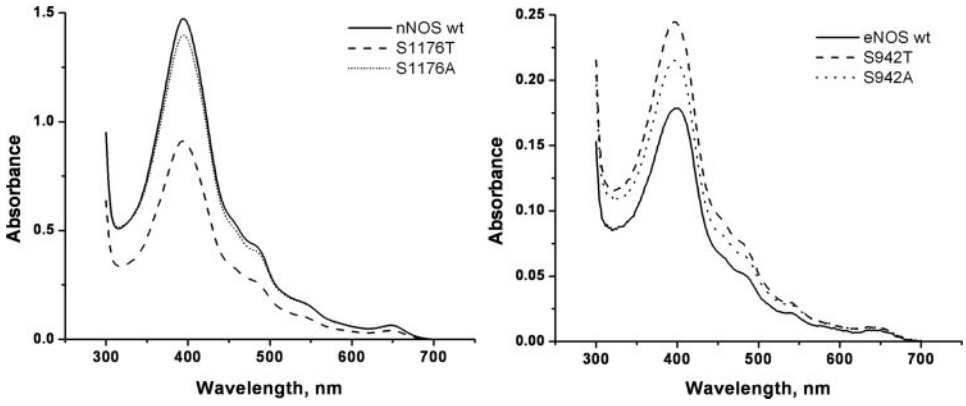

FIGURE 3. **Absolute spectra of NOSs.** The figure shows the absolute spectra of both nNOS and eNOS wild type (*wt*) (*solid line*) and their serine to threonine mutants (*dashed line*) and serine to alanine mutants (*dotted line*) for comparison.

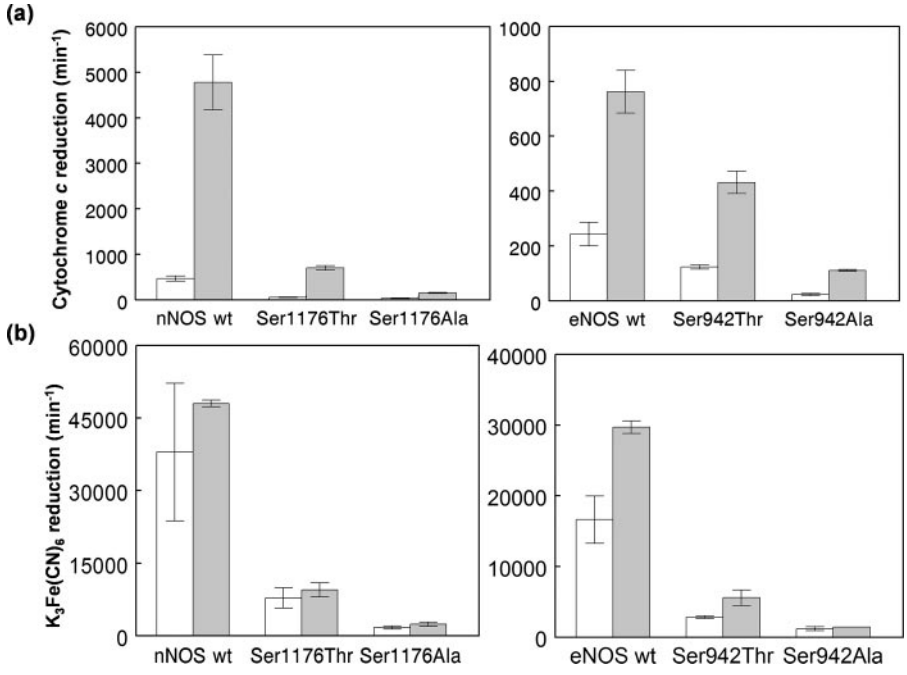

FIGURE 4. **Reductase activities of wild-type nNOS, wild type eNOS, and serine mutants.** *a*, cytochrome *c* reductase activity. Turnover numbers for cytochrome *c* reduction were measured using 20 nM (nNOS) or 50 nM (eNOS) of enzyme, both in the absence and presence of Ca^{2+}/CaM as described under "Experimental Procedures." The *open bars* represent rates in the absence of Ca^{2+}/CaM, and *filled bars* show rates in its presence. Data shown represent the average of three or more independent experiments performed with two or more independent protein purifications. The wild type (*wt*) and mutant proteins for each isoform were expressed and purified simultaneously to minimize errors between purifications. *b*, potassium ferricyanide reduction. Rates of potassium ferricyanide reduction were measured using 20 nM (nNOS) or 50 nM (eNOS) enzyme, both in the absence and presence of Ca^{2+}/CaM as described under "Experimental Procedures." *Open bars*, rates in the absence of Ca^{2+}/CaM; *filled bars*, rates in its presence. Data shown represent the average of three or more independent experiments performed with two or more independent protein purifications. The wild type and mutant proteins for each isoform were expressed and purified simultaneously to minimize errors between purifications.

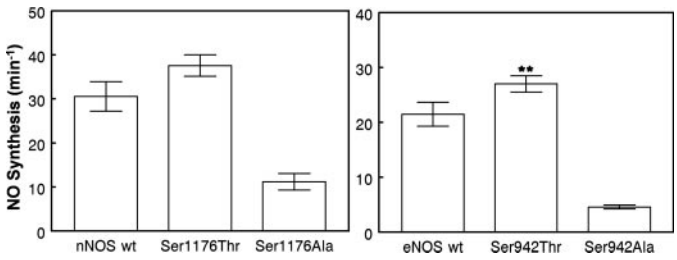

FIGURE 5. **Rate of nitric oxide production by wild-type nNOS and eNOS and their serine mutants.** Rates of NO production were measured as described under "Experimental Procedures" using the hemoglobin capture assay. Data shown represent the average of three or more independent experiments done with two independent protein purifications. The wild type (*wt*) and mutant proteins for each isoform were expressed and purified simultaneously to minimize the error between purifications. **, $p < 0.05$ was obtained for eNOS S942T compared with the eNOS wt (the *p* value was determined from two-tailed Student's *t* test).

much larger diminution in the activity was measured in the case of nNOS S1176A. A ~22-fold decrease from the wild type activity was observed for nNOS S1176A in the absence of Ca^{2+}/CaM (37,800 min^{-1} *versus* mutant activity 1700 min^{-1}), and a ~20-fold decrease in the presence of Ca^{2+}/CaM (48,000 min^{-1} *versus* mutant activity 2400 min^{-1}) was observed. In the case of the eNOS S942T mutation, the measured activity in the absence of Ca^{2+}/CaM was ~6-fold less than the wild type eNOS activity (17,000 *versus* 2900 min^{-1}) and ~5.5-fold less in the presence of Ca^{2+}/CaM (30,000 *versus* 5600 min^{-1}). The alanine substitution showed a much larger decrease in the activity as compared with the threonine substitution. In the absence of Ca^{2+}/CaM, the eNOS S942A mutant showed a ~14-fold decrease in the $K_3Fe(CN)_6$ reduction (wild type rate 17,000 min^{-1} *versus* mutant rate 1200 min^{-1}) and ~20-fold decrease in the presence of Ca^{2+}/CaM (wild type rate 30,000 min^{-1} *versus* mutant rate 1400 min^{-1}) as compared with the wild type activity. For nNOS WT, the K_m for ferricyanide was determined to be 1–1.5 mM, similar to that reported by Roman *et al.* (42) for S1176T, 0.5–1.0 mM, and for S1176A, 0.3–0.7 mM. However, the apparent K_m values for ferricyanide for eNOS wild type and the mutants were lowered compared with the nNOS and the mutants. For eNOS wild type, the K_m for ferricyanide was 0.4–0.6 mM, for S942T, it was 0.25 mM, and for S942A, it was 0.05 mM. In summary, the decrease in the rate of potassium ferricyanide reduction for nNOS and eNOS resulting from both alanine and threonine substitutions implies that the mutation of the serine spatially contiguous to FAD affects electron transfer from NADPH to/from FAD.

NO Production—Substitution of serine with threonine or alanine inhibited the rate of electron flow through the flavin domain as seen by the reduction of external electron acceptors, such as cytochrome *c* and ferricyanide, which are *not* the physiological partners. To determine the effect of the mutation on enzymatic activity, which involves transfer of electrons to the heme domain, the rate of NO production by these mutants was measured and compared with that of the wild type enzymes (Fig. 5). The rate of NO production in the serine to alanine mutation, in both nNOS and eNOS, is significantly lower than that of the wild type proteins. The alanine substitution *reduced* the rate of NO production by 2.7- and 4.7-fold for nNOS and eNOS, respectively. However, when serine was replaced with threonine, an equal or a slightly higher rate of NO production was consistently observed for both nNOS and eNOS in multiple preparations.

Rapid Kinetics Measurement of Flavin Reduction—To examine the effect of these mutations on the initial rate of flavin reduction, the rates for both wild type and mutant proteins were measured using stopped-flow spectrophotometry (Fig. 6). The kinetic traces of flavin reduction can be fitted to either a biphasic or a triphasic equation within the measured time frame (0.5 or 2 s), consistent with published work (34, 47).

As previously pointed out, observed changes in the rapid kinetics of NOS flavin-mediated electron transfer represent

transitions between pathway segments composed of states in rapid equilibrium, not transitions between individual states (47). The initial rapid phase of flavin bleaching corresponds to loss of 485 nm absorbance due to the establishment of rapid equilibrium between the initial NADPH complex of the oxidized enzyme, the FAD charge transfer complex with NADPH, and the $FADH_2$ state with $NADP^+$ bound.

The data clearly show that both the S1176T and S1176A mutants have markedly slower rates of reduction by NADPH in comparison with wild type nNOS in the presence and absence of Ca^{2+}/CaM (Table 1). In both cases, the slower rates are likely to be associated with processes limited or gated by the binding and release of pyridine nucleotides (see "Discussion") and cannot be solely attributed to the altered thermodynamics of redox reactions.

Furthermore, unlike the fast phase of reduction of wild type nNOS, the fast phase of both the serine mutants is at most minimally influenced by Ca^{2+}/CaM activation. In contrast, the slow phase of S1176T is stimulated to a similar degree as wild type, but S1176A shows a modest 2-fold increase. Similar effects with wild type eNOS and mutations of the cognate Ser-942 residue to threonine or alanine were observed (data not shown).

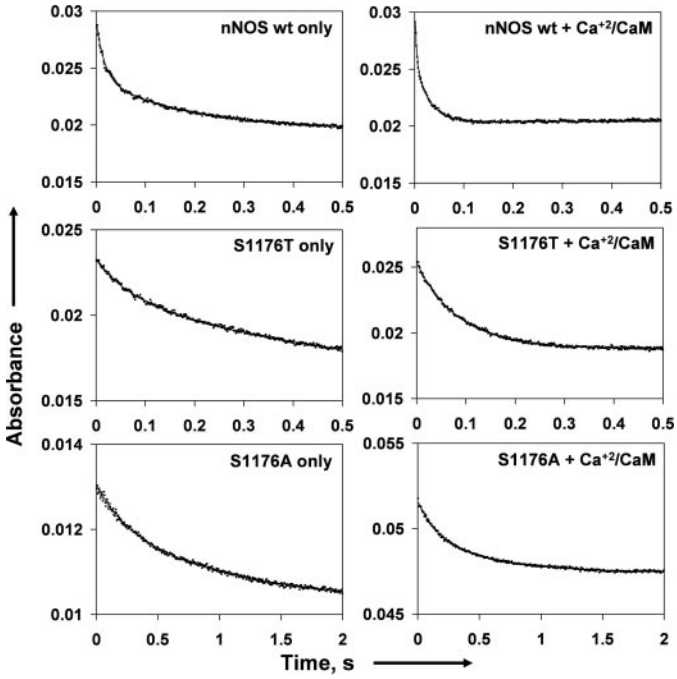

FIGURE 6. **Rapid kinetics measurements for wild type nNOS and its serine mutants.** The *traces* show the rapid kinetics measurements for nNOS wild type and its threonine and alanine mutants in the presence and absence of Ca^{2+}/CaM. The measured data (*rough line*) was fitted (*smooth line*) to a double exponential equation using the vendor-supplied program. Each *trace* is an average of three independent measurements.

Redox Potential Measurements—To probe the underlying mechanism of the role of the serine in the FAD domain, midpoint potentials were measured for various flavin redox states (Table 2). Fig. 7*a* shows the changes in absorbance of nNOS S1176T and S1176A at 600 and 650 nm at various potentials during titration. This wavelength region was chosen, since it contains information regarding all five one-electron E_m values due to flavin semiquinones and high spin ferriheme (37, 48). Simulations were performed to obtain the midpoint potential of these states (Fig. 7*a*, *lower panels*). Similarly, Fig. 7*b* shows the change in absorbance of eNOS S942T and S942A during titration at 600 and 650 nm. Simulation of titration spectra at other wavelengths was also generated as shown in Fig. 8. Shown in Fig. 8*a* are *actual spectra* obtained with nNOS S1176T (360–440 nm). Fig. 8*b* shows the absorbance changes as a function of changes in potential plotted as an increase at 390 nm and a decrease at 414 nm. Fig. 8*c* shows the simulated data for various flavin redox state components of nNOS S1176A obtained at 480 nm. These three different wavelengths were chosen to further support the potentials generated by simulations performed at 600 and 650 nm (Table 2). First of all, the heme Soret band was chosen to confirm heme potentials. All four mutants showed very similar Soret band signatures (Fig. 8*a*). The shift of the Soret peak from 414 to 390 nm can be clearly observed as the enzyme reoxidizes, and the plot of peak heights at these wavelengths confirms the single component E_m for heme to be around −300 mV. It is worth mentioning that although oxidized and reduced flavins have optical contribution in the Soret region, the contribution of heme is dominant. At 414 nm, almost the entire change is due to the formation of ferroheme, whereas at 390 nm, reduction of FMN contributes to the spectrum of wild type enzyme at high potential, and reduction of FAD contributes at potentials where the heme redox state is changing. Verification of flavin potentials was done by simulations at 480 nm, a region on the shoulder of the heme Soret, but with flavin species responsible for most of the optical changes. Using nNOS S1176A as an example, the intensity of the 480 nm band was simulated with contributions from oxidized flavins, and the blue neutral semiquinones of both FAD and FMN (Fig. 8*c*). For both the nNOS and eNOS alanine mutants at this position, the FAD semiquinone is too unstable to allow the determination of individual one-electron potentials and can be omitted from the simulations. Although the semiquinone of FAD (*dashed line*) cannot be readily monitored, the formation of oxidized FAD (*dashed and dotted line*) was visible together with the stabilized FMN semiquinone (*dotted line*), allowing the

TABLE 1

Rapid kinetic measurement of flavin reduction

Rates are measured in s^{-1}. The values within parentheses indicate the percentage contribution of the fast and slow phases of the kinetics.

Enzyme	Without Ca^{2+}/calmodulin		With Ca^{2+}/calmodulin	
	Fast phase	Slow phase	Fast phase	Slow phase
	s^{-1}		s^{-1}	
nNOS wild type	57.4 ± 0.7 (51%)	4.95 ± 0.45 (49%)	293 ± 30 (53%)	31.05 ± 6.55 (47%)
nNOS S1176T	15.5 ± 3.6 (30%)	2.02 ± 0.4 (70%)	13.8 ± 0.3 (46%)	9.7 ± 0.77 (54%)
nNOS S1176A	3.9 ± 0.6 (33%)	0.9 ± 0.1 (67%)	6.2 ± 0.4 (48%)	1.8 ± 0.1 (52%)

TABLE 2
Midpoint potentials of different redox centers

	FMN ox/sq	FMN sq/hq	FAD ox/sq	FAD sq/hq	Heme single	Heme high	Heme low
	mV	*mV*	*mV*	*mV*	*mV*	*mV*	*mV*
nNOS wild type	−120	−220	−250	−260	−290	−250	−350
nNOS S1176T	−120	−220	−240	−300	−300		
nNOS S1176A	>40[a]	−240		−205[b]	−290		
eNOS Wild type	−105	−240	−230	−260	−280	−260	−350
eNOS S942T	−100	−240	−230	−240	−280		
eNOS S942A	>80[a]	−230		−200[b]	−280		

[a] Values signify positive potentials out of the mediated titration region.
[b] Due to the unstable FAD semiquinone in the alanine mutants, the FAD ox/sq state cannot be monitored clearly in order to give accurate individual FAD potentials. Since $FADH_2$ oxidation can be successfully simulated by treating it as a $2e^-$ process; the $2e^-$ value is given.

measurement of the two-electron potential for FAD; the first one-electron reduction of FAD must be at least 60 mV more negative than the second one-electron reductive step. The oxidized FMN is not shown in the simulation due to the very high potential for the FMN/$FMNH^\bullet$ transition. Similar transitions were also observed in the simulation of the 650 nm band (Fig. 7*a*). These data are in complete agreement with the data in Table 2. Both nNOS and eNOS threonine mutants possess very similar redox potentials in comparison with respective wild types. Both of the threonine mutant simulation plots show trends similar to that of wild type protein, as reported by Gao *et al.* (37). A considerable difference was observed for the alanine mutants of both nNOS and eNOS. Disruption of the hydrogen bonding network near FAD by alanine *increased* the redox potential of the $FADH^\bullet/FADH_2$ couple ~50 mV. The most striking difference was noticed for the FMN/$FMNH^\bullet$ couple for the alanine mutant of both nNOS and eNOS, which made this redox couple 160 and 185 mV more positive compared with the wild type, respectively. The exact potential for the FMN/$FMNH^\bullet$ transition in this mutant is too positive to be determined accurately using our mediated titration system. Fig. 9, *a* and *b*, show comparative plots of midpoint potentials of the different redox centers of wild type and mutant cNOSs. Unlike the wild type or the threonine mutants, these plots show that the FMN semiquinone of alanine mutants is stable even at very high potential.

Flavin reduction by NADPH and reoxidation of the wild type and mutant proteins were measured at 485 nm as described earlier (12, 13). The threonine mutants of both nNOS and eNOS clearly showed a fully reduced state, which reoxidized gradually upon depletion of NADPH. Similar kinetics have been reported earlier for wild type proteins (12, 13). On the other hand, alanine mutants that cannot make some critical hydrogen bonds demonstrated different kinetics, showing a much less stable reduced flavin state, which reoxidized rapidly (data not shown).

DISCUSSION

Evolution of FAD and FMN binding sites has allowed development of unique catalytic properties in electron transferring enzymes (49, 50). Flavin cofactors often participate in intricate hydrogen bonding systems. Conserved hydrogen bonding networks involving serine (Ser-457 of rat CYPOR, Ser-1176 of rat nNOS), aspartate (Asp-675 of CYPOR, Asp-1393 of nNOS), and cysteine (Cys-630 of CYPOR, Cys-1349 of nNOS) flank FAD in NOS and CYPOR (Fig. 2) (16–18). Ser-1176 is within hydrogen bonding distance of N5 and O4 of FAD and Asp-1393. A hydride transfer mechanism for CYPOR and homologues has been proposed, envisioning important roles for the serine OH group and its neighbors. Ser-457 of CYPOR (22) and Ser-96 in ferredoxin-$NADP^+$ reductase (39) (FNR) were implicated in hydride transfer. Ser-457 mutants of CYPOR have low electron transfer rates to external acceptors, but K_m values for NADPH are normal.

Here we studied the role of nNOS Ser-1176 and its eNOS cognate, Ser-942, by mutation to threonine or alanine. Flavin reduction rates and redox potentials were affected, and $K_3Fe(CN)_6$ and cytochrome *c* reduction were impaired. In stopped-flow experiments, both major phases of flavin absorbance changes are slower in the mutants.

Knight and Scrutton (47) pointed out difficulties in assigning kinetics phases in stopped flow experiments to specific processes, assigning phases to rapid equilibrium segments rather than specific states. These phases are likely to be limited by pyridine nucleotide binding/release and/or associated local conformational changes, which gate electron transfer processes. Their uncoupling of kinetic phases from FAD and FMN reduction is an important contribution.

The majority of the 485 nm absorbance change is most likely due to the conversion of FAD to the charge transfer complex and the reduced state, both of which are reflected in the phase I rate in Table 1, whereas the second or subsequent kinetic phases probably reflect shifts in component equilibria.

Both S1176T and S1176A exhibit slower rates of phase I conversion. Midpoint potential alone cannot account for this, since the reduction of FAD by NADPH is favorable. The limiting process thus cannot be only electron transfer, and the disruptive nature of the mutants suggests that it is also the formation of the charge transfer complex with the NADPH. In wild type nNOS, calmodulin affects both the initial phase, limited by NADPH binding, and the second slower phase, probably limited by $NADP^+$ release or internal processes, such as conformational changes (52). It is conceivable that disruption of the precise environment and the precise hydrogen-bonding network by substitution of threonine or alanine for serine alters binding and release of pyridine nucleotides; our results further indicate that this also negates the effect of Ca^{2+}/CaM on the initial binding of NADPH.

The structural basis for the altered kinetics has several components. The alanine mutants lose side chain hydrogen bonding to N5 of FAD, and potential backbone hydrogen bonding is

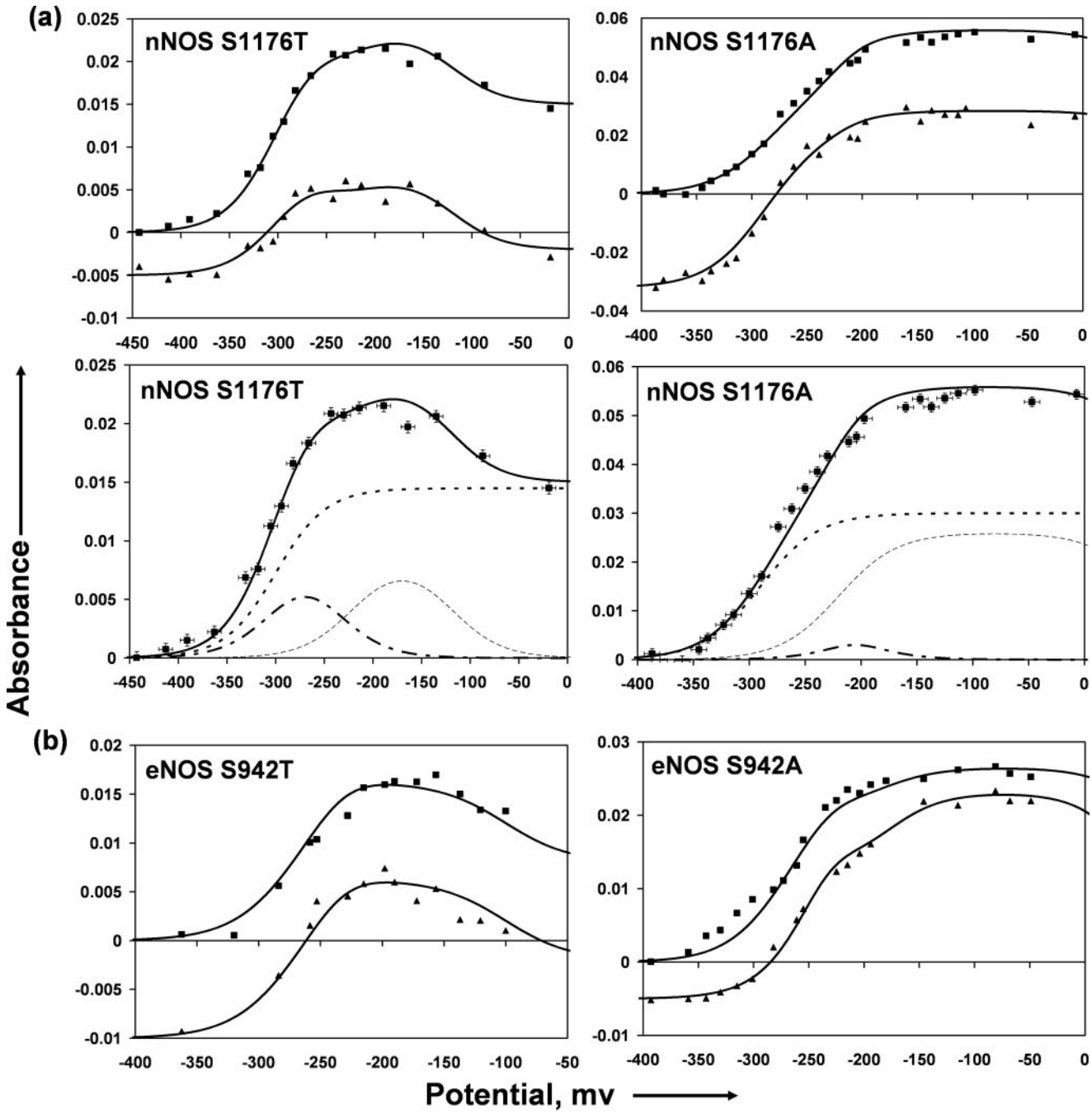

FIGURE 7. **Redox titrations of serine mutants of nNOS and eNOS.** Intensities of 600 nm (■) and 650 nm (▲) bands, during redox titration, of nNOS S1176T and S1176A mutants (*a*) and eNOS S942T and S942A (*b*) were plotted against the potential, and data were simulated (*solid line*) for flavin redox states using the Nernst equation (37). Deconvolution of nNOS S1176T and nNOS S1176A at 650 nm (*a*, *bottom panels*). Three components, the high spin ferriheme charge transfer band (*dotted line*), the blue neutral semiquinones of FMN (*thin dashed line*), and FAD (*dashed and dotted line*), add up to give rise to the composite curve (*solid line*), which simulates experimental data points (*filled black squares*) to ±10–20 mV accuracy. The base line has been corrected by subtraction of the most reduced spectrum. Fitting parameters for S1176T are as follows: FAD, $E_{ox/sq} = -240$, $E_{sq/hq} = -300$, $c^*\epsilon = 0.02$; FMN, $E_{ox/sq} = -120$, $E_{sq/hq} = -220$, $c^*\epsilon = 0.02$; heme, $E_m = -300$, $c^*\epsilon = 0.012$; fitting parameters for S1176A are as follows: FAD, $E_{ox/sq} = -240$, $E_{sq/hq} = -170$, $c^*\epsilon = 0.02$; FMN, $E_{ox/sq} > 40$, $E_{sq/hq} = -240$, $c^*\epsilon = 0.02$; heme, $E_m = -290$, $c^*\epsilon = 0.012$. Deconvoluted curves for eNOS mutant simulation gave similar results (data not shown).

perturbed by disrupting the Ser-1176–Asp-1393 side chain hydrogen bond. Smaller rate reductions were observed in the threonine mutants, which can still form a hydrogen bond with the side chain of Asp-1393. Analysis of the wild type crystal structure suggests that the space surrounding Ser-1176 is sterically restricted and cannot easily accommodate an additional methylene. To accommodate the additional group, the local backbone and neighboring strands must be relaxed. Changes in the FAD environment can influence electron transfer without compromising the structural integrity of the protein.

Although electron transfer to external acceptors is reduced in the threonine mutants, NO production is normal. Threonine mutants of both nNOS and eNOS have midpoint potentials comparable with those of wild type enzymes (Table 2). In wild-type NOS, electron transfer to the heme domain is rate-limit-

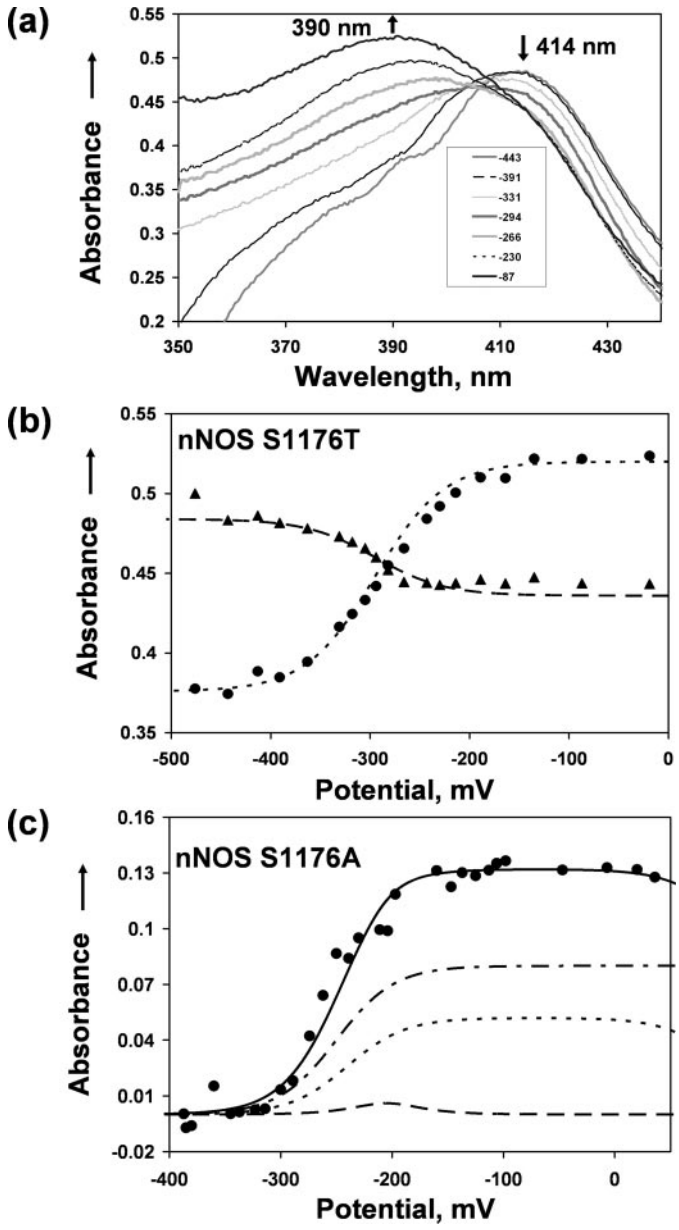

FIGURE 8. **Titration spectra of S1176T in the Soret region and simulation of S1176A data at 480 nm.** *a*, actual spectra of S1176T around the Soret region (360–440 nm) at different potentials are overlaid. *b*, plot of the absorbance changes at wavelengths 390 nm (■) and 414 nm (▲) *versus* potentials. The *lines* through the data points are the simulated curves. *c*, absorbances at 480 nm (●) at different potentials during titration of nNOS S1176A mutant were simulated using the redox potentials obtained from the simulations at 600 and 650 nm. The *fitted line* (*solid line*) is deconvoluted to show the contributing components, FADox (*dotted and dashed line*), FADsq (*dashed line*), and FMNsq (*dotted line*).

ing, and apparently the conservative serine/threonine substitution does not affect the limiting step. The alanine mutant, on the other hand, exhibits reduced NO production, indicating that electron transfer to the heme domain is slow, as expected from the redox potentials; the higher potential of $FADH^{\bullet}/FADH_2$ couple makes the reduction of the $FMNH^{\bullet}$ semiquinone unfavorable (Table 2).

Loss of the hydrogen bonding pattern near FAD, which plays an important role during catalysis in CYPOR (41), appears to influence the environment of FAD in alanine mutants and may interfere with the CaM-mediated release of the NADPH-dependent conformational lock (52). Conformational lock release enables the FMN domain to interact with the heme domain during catalysis, and with cytochrome *c in vitro* (53).

There are several mechanisms by which amino acid residues can modify flavin electrochemistry. Ring stacking with the shielding residue inhibits formation of the isoalloxazine chair conformation, lowering the potentials. Hydrogen bond donors interacting with the isoalloxazine ring generally raise the potentials, and hydrogen bond acceptor interactions lower the potentials (54). Electrostatic interactions with charged residues and solvent interactions are additional factors.

Hubbard *et al.* (41) proposed a model for catalysis by CYPOR, which invokes formation and dissociation of hydrogen bonds to the side chain OH of serine, depending upon the redox state of FAD and the binding of NADPH, thus cyclically altering flavin midpoint potentials. With FAD oxidized, the Ser-457 side chain is hydrogen-bonded to Asp-675. NADPH binding and formation of the charge transfer complex produces an additional Ser-457 hydrogen bond with NADPH. FAD reduction severs the NADPH and Ser-OH hydrogen bond, and a FAD/Ser-OH bond is formed. Reoxidation of FAD restores the original state. Crystal structures of oxidized nNOS reductase domains (17, 18) show the Ser-1176 side chain within hydrogen-bonding distance of Asp-1393, the Asp-675 cognate, but unlike CYPOR, the Ser-1176 backbone nitrogen is also within hydrogen-bonding distance of FAD N5.

Since the midpoint potential of the alanine mutant was raised rather than lowered, the effects of the alanine substitution cannot be attributed to a direct interaction with the 1176 side chain but must be the result of repositioning of the backbone, freeing of Asp-1393, or conformational effects within the FAD site. Increased interaction of the Ser-1176 backbone with isoalloxazine positions would be expected to favor reduced and semiquinone states over oxidized states, as long as N5 itself is not protonated, because of increased electron density in the isoalloxazine ring. Loss of the Asp-1393–Ser-1176 side chain hydrogen bond might stabilize semiquinone and reduced forms relative to oxidized states, if the orientation of the Ser-1176 peptide nitrogen were more favorable in the mutant. The increased midpoint potential of the $FADH^{\bullet}/FADH_2$ is consistent with this scenario. Similar effects could also be attributed to changes in the position of the nearby shielding residue (Phe-1395) because of the loss of the Asp-1393–Ser-1176 constraint (Fig. 2).

The alanine mutations have additional unexpected effects on FMN, producing a higher potential nonphysiological one-electron couple ($FMN/FMNH^{\bullet}$) (Table 2). We initially assigned the additional stabilized semiquinone to FAD, since the mutation was in the FAD region. However, this assignment does not readily account for titration of the 605 and 485 nm absorbances and still requires that the FMN couples change to reduce the contribution of the FMN semiquinone. Furthermore, the alanine mutants are able to transfer electrons and can undergo catalytic turnover. A very stable FAD semiquinone would create a kinetic bottleneck, preventing electron flow from $FADH^{\bullet}$ to FMN; the alternative unstable FAD semiquinone produces a

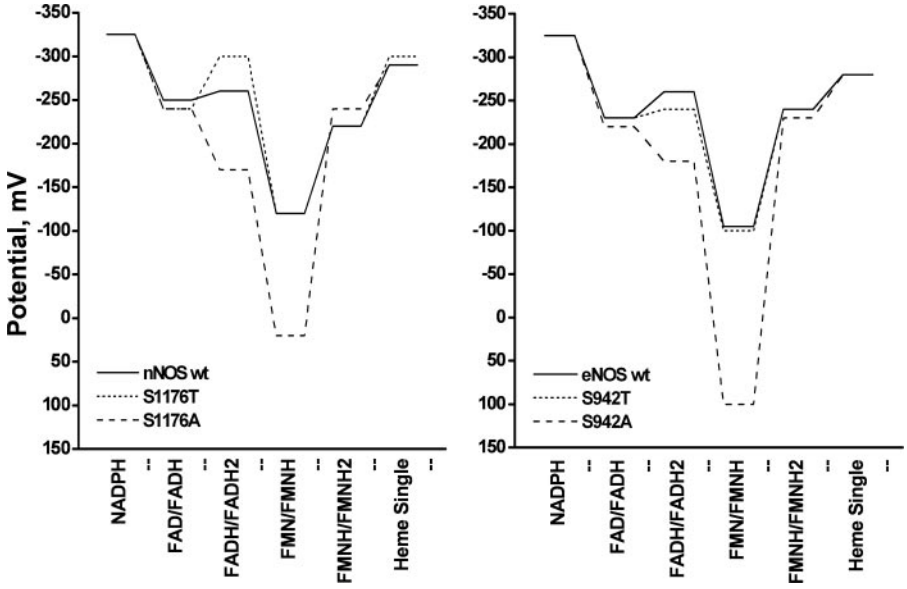

FIGURE 9. **Overlay of redox potentials of NADPH, heme, and different flavin redox states of nNOS and eNOS wild type (*wt*) and their serine mutants.** A step graph showing the redox potentials of different redox centers of wild type (*solid line*), threonine mutants (*dotted line*), and alanine mutants (*dashed line*) of both nNOS (*a*) and eNOS (*b*).

much less severe uphill step. These considerations indicate that the stable semiquinone is FMNH$^{\bullet}$. Since neither Ser-1176 nor Asp-1393 interacts directly with FMN, such an effect must be transmitted through the protein to the adjacent FMN binding site.

The altered flavin redox potentials mandate that the catalytic cycle of the S1176A type mutants will be affected at multiple points. The reduced ability of the mutants to form the charge transfer complex hinders FAD reduction, although the potentials are favorable for electron transfer from NADPH, leading to slower rates in rapid kinetics experiments and $K_3Fe(CN)_6$ reduction in alanine and threonine mutants.

It is intriguing that NO production by threonine mutants is comparable with that of wild type NOS, but flavoprotein-mediated reductase activity is impaired. During catalysis, donation of electrons by FMN to the oxygenase domain is rate-limiting for NO production. NADPH oxidation occurs in a "closed state" in which FMN interacts directly with the FAD domain, but the FMN domain must then be released from the reductase complex to initiate interactions with the oxygenase domain *or* artificial acceptors (relaxed state) (52, 55). FMN domain release is rate-limiting for cytochrome *c* reduction, but NO production depends on formation of a state in which the FMN domain interacts with the oxygenase domain (53).

In the threonine mutants, the extra methyl group in a sterically constrained environment perturbs the backbone and may decrease the rate of release of the FMN domain. Slower detachment of the FMN domain decreases the rate of cytochrome *c* reduction, which is relatively rapid. In the much slower NO synthesis reactions, reductase function of the threonine mutant enzyme is sufficient to support NO synthesis at wild type rate, and the rate of association of FMN domain with oxygenase domain may be enhanced. A small conformational change associated with the threonine mutant does not decrease NO synthesis and may even slightly increase it. $K_3Fe(CN)_6$ reduction decreases as expected, because the closed (input) conformation of the reduced enzyme can reduce $K_3Fe(CN)_6$. An interesting outcome of this analysis is that the majority of solution conformational/redox states observed during electron transfer to $K_3Fe(CN)_6$, cytochrome *c*, and the oxygenase domain for NO production are different. Therefore, it may be possible to trap kinetically an intermediate of the enzyme in which the FMN domain is neither associated with the FAD domain nor with the oxygenase domain.

Here we have shown that the conserved serine residue near FAD in the constitutive NOS isoforms plays an important role in catalysis. The mutational studies reported here and elsewhere highlight differences in the microenvironment of the flavins in groups of related proteins introduced during protein evolution.

Acknowledgment—We thank Dr. Christopher C. Marohnic for helpful discussions and for generating the structure figure.

REFERENCES

1. Roman, L. J., Martásek, P., and Masters, B. S. S. (2002) *Chem. Rev.* **102,** 1179–1190
2. Stuehr, D. J., Santolini, J., Wang, Z. Q., Wei, C. C., and Adak, S. (2004) *J. Biol. Chem.* **279,** 36167–36170
3. Moncada, S., and Higgs, A. (1993) *N. Engl. J. Med.* **329,** 2002–2012
4. Stuehr, D. J., Cho, H. J., Kwon, N. S., Weise, M. F., and Nathan, C. F. (1991) *Proc. Natl. Acad. Sci. U. S. A.* **88,** 7773–7777
5. Li, H., Shimizu, H., Flinspach, M., Jamal, J., Yang, W., Xian, M., Cai, T., Wen, E. Z., Jia, Q., Wang, P. G., and Poulos, T. L. (2002) *Biochemistry* **41,** 13868–13875
6. Flinspach, M., Li, H., Jamal, J., Yang, W., Huang, H., Silverman, R. B., and Poulos, T. L. (2004) *Biochemistry* **43,** 5181–5187
7. Raman, C. S., Li, H., Martásek, P., Kral, V., Masters, B. S. S., and Poulos, T. L. (1998) *Cell* **95,** 939–950
8. Fischmann, T. O., Hruza, A., Niu, X. D., Fossetta, J. D., Lunn, C. A., Dolphin, E., Prongay, A. J., Reichert, P., Lundell, D. J., Narula, S. K., and Weber, P. C. (1999) *Nat. Struct. Biol.* **6,** 233–242
9. Crane, B. R., Arvai, A. S., Ghosh, D. K., Wu, C., Getzoff, E. D., Stuehr, D. J., and Tainer, J. A. (1998) *Science* **279,** 2121–2126
10. Bredt, D. S., Hwang, P. M., Glatt, C. E., Lowenstein, C., Reed, R. R., and Snyder, S. H. (1991) *Nature* **351,** 714–718
11. Salerno, J. C., Harris, D. E., Irizarry, K., Patel, B., Morales, A. J., Smith, S. M., Martásek, P., Roman, L. J., Masters, B. S. S., Jones, C. L., Weissman, B. A., Lane, P., Liu, Q., and Gross, S. S. (1997) *J. Biol. Chem.* **272,** 29769–29777
12. Roman, L. J., Martásek, P., Miller, R. T., Harris, D. E., de La Garza, M. A., Shea, T. M., Kim, J. J., and Masters, B. S. S. (2000) *J. Biol. Chem.* **275,** 29225–29232
13. Roman, L. J., Miller, R. T., de La Garza, M. A., Kim, J. J., and Masters, B. S. S. (2000) *J. Biol. Chem.* **275,** 21914–21919
14. Lane, P., and Gross, S. S. (2002) *J. Biol. Chem.* **277,** 19087–19094
15. Jáchymová, M., Martásek, P., Panda, S., Roman, L. J., Panda, M., Shea,

T. M., Ishimura, Y., Kim, J. J., and Masters, B. S. (2005) *Proc. Natl. Acad. Sci. U. S. A.* **102,** 15833–15838
16. Wang, M., Roberts, D. L., Paschke, R., Shea, T. M., Masters, B. S. S., and Kim, J. J. (1997) *Proc. Natl. Acad. Sci. U. S. A.* **94,** 8411–8416
17. Zhang, J., Martásek, P., Paschke, R., Shea, T., Masters, B. S. S., and Kim, J. J. (2001) *J. Biol. Chem.* **276,** 37506–37513
18. Garcin, E. D., Bruns, C. M., Lloyd, S. J., Hosfield, D. J., Tiso, M., Gachhui, R., Stuehr, D. J., Tainer, J. A., and Getzoff, E. D. (2004) *J. Biol. Chem.* **279,** 37918–37927
19. Shen, A. L., Porter, T. D., Wilson, T. E., and Kasper, C. B. (1989) *J. Biol. Chem.* **264,** 7584–7589
20. Sem, D. S., and Kasper, C. B. (1992) *Biochemistry* **31,** 3391–3398
21. Shen, A. L., and Kasper, C. B. (1995) *J. Biol. Chem.* **270,** 27475–27480
22. Shen, A. L., and Kasper, C. B. (1996) *Biochemistry* **35,** 9451–9459
23. Shen, A. L., and Kasper, C. B. (2000) *J. Biol. Chem.* **275,** 41087–41091
24. Porter, T. D., and Kasper, C. B. (1986) *Biochemistry* **25,** 1682–1687
25. Michael, S. F. (1994) *BioTechniques* **16,** 410–412
26. Martásek, P., Liu, Q., Liu, J., Roman, L. J., Gross, S. S., Sessa, W. C., and Masters, B. S. S. (1996) *Biochem. Biophys. Res. Commun.* **219,** 359–365
27. Roman, L. J., Sheta, E. A., Martásek, P., Gross, S. S., Liu, Q., and Masters, B. S. S. (1995) *Proc. Natl. Acad. Sci. U. S. A.* **92,** 8428–8432
28. Zhang, M., and Vogel, H. J. (1994) *Biochemistry* **33,** 1163–1171
29. Paul, K. G., Theorell, H., and Akeson, A. (1953) *Acta Chem. Scand.* **7,** 1284
30. Rieske, J. S. (1967) *Methods Enzymol.* **10,** 488–493
31. Faeder, E. J., and Siegel, L. M. (1973) *Anal. Biochem.* **53,** 332–336
32. Aliverti, A., Curti, B., and Vanoni, M. A. (1999) in *Flavoprotein Protocols* (Chapman, S. K., and Reid, G. A., eds) pp. 9–23, Humana Press, Totowa, NJ
33. Masters, B. S. S., Williams, C. H. J., and Kamin, H. (1967) *Methods Enzymol.* **10,** 565–573
34. Miller, R. T., Martásek, P., Omura, T., and Masters, B. S. S. (1999) *Biochem. Biophys. Res. Commun.* **265,** 184–188
35. Kelm, M., Feelisch, M., Spahr, R., Piper, H. M., Noack, E., and Schrader, J. (1988) *Biochem. Biophys. Res. Commun.* **154,** 236–244
36. Dutton, P. L. (1978) *Methods Enzymol.* **54,** 411–435
37. Gao, Y. T., Smith, S. M., Weinberg, J. B., Montgomery, H. J., Newman, E., Guillemette, J. G., Ghosh, D. K., Roman, L. J., Martásek, P., and Salerno, J. C. (2004) *J. Biol. Chem.* **279,** 18759–18766
38. Dunford, A. J., Marshall, K. R., Munro, A. W., and Scrutton, N. S. (2004) *Eur. J. Biochem.* **271,** 2548–2560
39. Aliverti, A., Bruns, C. M., Pandini, V. E., Karplus, P. A., Vanoni, M. A., Curti, B., and Zanetti, G. (1995) *Biochemistry* **34,** 8371–8379
40. Kimura, S., Kawamura, M., and Iyanagi, T. (2003) *J. Biol. Chem.* **278,** 3580–3589
41. Hubbard, P. A., Shen, A. L., Paschke, R., Kasper, C. B., and Kim, J. J. (2001) *J. Biol. Chem.* **276,** 29163–29170
42. Roman, L. J., McLain, J., and Masters, B. S. S. (2003) *J. Biol. Chem.* **278,** 25700–25707
43. Alexander, L. M., Hersh, L. B., and Masters, B. S. (1980) in *Microsomes, Drug Oxidations, and Chemical Carcinogenesis* (Coon, M. J., Conney, A. H., Estabrook, R. W., Gelboin, H. V., Gillette, J. R., and O'Brien, P. J., eds) pp. 285–288, Academic Press, Inc., New York
44. Vermilion, J. L., Ballou, D. P., Massey, V., and Coon, M. J. (1981) *J. Biol. Chem.* **256,** 266–277
45. Kurzban, G. P., Howarth, J., Palmer, G., and Strobel, H. W. (1990) *J. Biol. Chem.* **265,** 12272–12279
46. Martásek, P., Miller, R. T., Roman, L. J., Shea, T., and Masters, B. S. S. (1999) *Methods Enzymol.* **301,** 70–78
47. Knight, K., and Scrutton, N. S. (2002) *Biochem. J.* **367,** 19–30
48. Ghosh, D. K., Holliday, M. A., Thomas, C., Weinberg, J. B., Smith, S. M. E., and Salerno, J. C. (2006) *J. Biol. Chem.* **281,** 14173–14183
49. Massey, V. (2000) *Biochem. Soc. Trans.* **28,** 283–296
50. Fraaije, M. W., and Mattevi, A. (2000) *Trends Biochem. Sci* **25,** 126–132
51. Karplus, P. A., Walsh, K. A., and Herriott, J. R. (1984) *Biochemistry* **23,** 6576–6583
52. Craig, D. H., Chapman, S. K., and Daff, S. (2002) *J. Biol. Chem.* **277,** 33987–33994
53. Roman, L. J., and Masters, B. S. S. (2006) *J. Biol. Chem.* **281,** 23111–23118
54. Faro, M., Gómez-Moreno, C., Stankovich, M. T., and Medina, M. (2002) *Eur. J. Biochem.* **269,** 2656–2661
55. Ghosh, D. K., and Salerno, J. C. (2003) *Front. Biosci.* **8,** d193–d209
56. Lamas, S., Marsden, P. A., Li, G. K., Tempst, P., and Michel, T. (1992) *Proc. Natl. Acad. Sci. U. S. A.* **89,** 6348–6352
57. Xie, Q. W., Cho, H. J., Calaycay, J., Mumford, R. A., Swiderek, K. M., Lee, T. D., Ding, A., Troso, T., and Nathan, C. (1992) *Science* **256,** 225–228
58. Ruettinger, R. T., Wen, L. P., and Fulco, A. J. (1989) *J. Biol. Chem.* **264,** 10987–10995
59. Ohgiya, S., Shinriki, N., Kamataki, T., and Ishizaki, K. (1994) *Biochim. Biophys. Acta* **1186,** 137–141
60. Pietrini, G., Carrera, P., and Borgese, N. (1988) *Proc. Natl. Acad. Sci. U. S. A.* **85,** 7246–7250
61. Leclerc, D., Wilson, A., Dumas, R., Gafuik, C., Song, D., Watkins, D., Heng, H. H., Rommens, J. M., Scherer, S. W., Rosenblatt, D. S., and Gravel, R. A. (1998) *Proc. Natl. Acad. Sci. U. S. A.* **95,** 3059–3064
62. Vaucheret, H., Vincentz, M., Kronenberger, J., Caboche, M., and Rouze, P. (1989) *Mol. Gen. Genet.* **216,** 10–15
63. Makino, K., Yokoyama, K., Kubota, Y., Yutsudo, C. H., Kimura, S., Kurokawa, K., Ishii, K., Hattori, M., Tatsuno, I., Abe, H., Iida, T., Yamamoto, K., Onishi, M., Hayashi, T., Yasunaga, T., Honda, T., Sasakawa, C., and Shinagawa, H. (1999) *Genes Genet. Syst.* **74,** 227–239
64. Suh, Y. A., Arnold, R. S., Lassegue, B., Shi, J., Xu, X., Sorescu, D., Chung, A. B., Griendling, K. K., and Lambeth, J. D. (1999) *Nature* **401,** 79–82
65. Dujon, B., Alexandraki, D., Andre, B., Ansorge, W., Baladron, V., Ballesta, J. P., Banrevi, A., Bolle, P. A., Bolotin-Fukuhara, M., Bossier, P., *et al.* (1994) *Nature* **369,** 371–378

The Role of a Conserved Serine Residue within Hydrogen Bonding Distance of FAD in Redox Properties and the Modulation of Catalysis by Ca^{2+}/Calmodulin of Constitutive Nitric-oxide Synthases

Satya Prakash Panda, Ying Tong Gao, Linda J. Roman, Pavel Martásek, John C. Salerno and Bettie Sue S. Masters

J. Biol. Chem. 2006, 281:34246-34257.
doi: 10.1074/jbc.M601041200 originally published online September 11, 2006
